UNCLASSIFIED

DTIC FILE COPY

4

SECURITY CLASSIFICATION OF THIS PAGE

REPORT DOCUMENTATION PAGE

1a. REPORT SECURITY CLASSIFICATION: Unclassified	1b. RESTRICTIVE MARKINGS: none
2a. SECURITY CL: N/A	DISTRIBUTION/AVAILABILITY OF REPORT: UNRESTRICTED
2b. DECLASSIFIC: N/A	
4. PERFORMING: BTI-A002	MONITORING ORGANIZATION REPORT NUMBER(S)
6a. NAME OF PERFORMING ORGANIZATION: Burton Technologies Inc.	6b. OFFICE SYMBOL (If applicable):
6c. ADDRESS (City, State and ZIP Code): 554 Pylon Drive, Raleigh, NC 27606	7a. NAME OF MONITORING ORGANIZATION: Office of Naval Research
8a. NAME OF FUNDING/SPONSORING ORGANIZATION: Office of Naval Research	8b. OFFICE SYMBOL (If applicable):
8c. ADDRESS (City, State and ZIP Code): 800 N. Quincy Street, Arlington, VA 22217-5000	7b. ADDRESS (City, State and ZIP Code): 800 N. Quincy Street, Arlington, VA 22217-5000
	9. PROCUREMENT INSTRUMENT IDENTIFICATION NUMBER: N00014-86-C-0836
	10. SOURCE OF FUNDING NOS.

PROGRAM ELEMENT NO.	PROJECT NO.	TASK NO.	WORK UNIT NO.

11. TITLE (Include Security Classification): Final Report

12. PERSONAL AUTHOR(S): Ralph A. Burton, R. Gaines Burton

13a. TYPE OF REPORT	13b. TIME COVERED	14. DATE OF REPORT (Yr., Mo., Day)	15. PAGE COUNT
Final	FROM 9/1/86 TO 8/31/88	10/25/88	

16. SUPPLEMENTARY NOTATION: N/A

17. COSATI CODES			18. SUBJECT TERMS (Continue on reverse if necessary and identify by block number)
FIELD	GROUP	SUB. GR.	

19. ABSTRACT (Continue on reverse if necessary and identify by block number)

The potential for eutectic alloys of Gallium in current collectors is examined. The focus of the program was on GaInSn alloy. Basic properties of the alloy are determined as well as oxide control and corrosion of copper. Designs for high current density current collectors are examined including novel hydrodynamic pads. Alloy handling problems and material compatibility are discussed.

DTIC ELECTE OCT 28 1988 S C E

20. DISTRIBUTION/AVAILABILITY OF ABSTRACT	21. ABSTRACT SECURITY CLASSIFICATION
UNCLASSIFIED/UNLIMITED ☐ SAME AS RPT. ☒ DTIC USERS ☐	UNCLASSIFIED

22a. NAME OF RESPONSIBLE INDIVIDUAL	22b. TELEPHONE NUMBER (Include Area Code)	22c. OFFICE SYMBOL
R. Gaines Burton	(919)-839-8287	

DD FORM 1473, 83 APR — EDITION OF 1 JAN 73 IS OBSOLETE. UNCLASSIFIED

SECURITY CLASSIFICATION OF THIS PAGE

REPORT BTI-A002

CONTROL OF SURFACE ATTACK BY GALLIUM ALLOYS

AUTHORS: RALPH A. BURTON
R. GAINES BURTON

BURTON TECHNOLOGIES INC
554 PYLON DRIVE
RALEIGH,NC 27606

OCTOBER 25,1988

CONTRACT No. N00014-86-C-0836

FINAL REPORT

PREPARED FOR:

OFFICE OF NAVAL RESEARCH
800 NORTH QUINCY STREET
ARLINGTON,VA 22217-5000

1. FOREWORD

This document summarizes the findings of a two-year research program undertaken to determine the feasibility for use of low melting, gallium based alloys in high-current density electrical slip rings. The research was sponsored by the United States Office of Naval Research under a Small Business Innovation Research, Phase II contract.

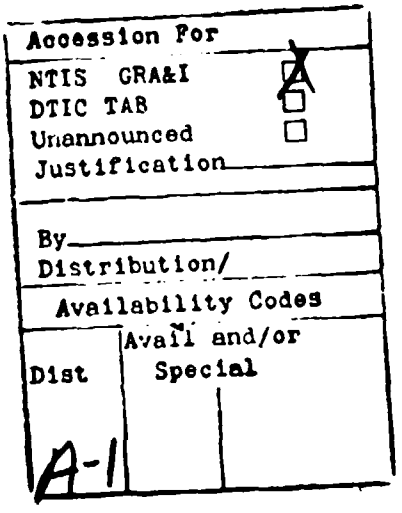

2. TABLE OF CONTENTS

3. LIST OF FIGURES

4. LIST OF TABLES

5. LIST OF SYMBOLS

B Length of bearing pad in direction of sliding

d Bore diameter for tube (m)

d_2 Diameter of drop where cut by datum plane (m)

e_1 Potential drop on reference resistor (mv)

e_2 Potential drop on column of alloy (mv)

F Horizontal force on bearing pad (N)

F_o Tangential force on pad at liftoff condition (N)

g Acceleration of gravity (m/sec^2)

G Parameter defined in Eq. (8.24)

K Dimensionless measure of pad tilt

L Length of column of alloy (cm)

m Mass collected (g)

M Hartmann number (dimensionless)

p Equivalent pressure drop on alloy column (N/cm^2)

Q Heat generation (watt)

r Radius of drop measured in a horizontal plane (m)

r_o Radius of drop at lowest point, in vertical plane (m)

$\underline{r}$ Resistivity of alloy (micro-ohm cm)

R Electrical resistance of film under pad (ohm)

R_1 Reference resistance (ohm), also inner radius of tube (m)

R_2 Column resistance (ohm), also outer radius of tube (m)

Re Reynolds number (dimensionless)

s Coordinate on drop surface measured on line of intersection with vertical plane

t Time required for efflux of m in viscometer (s)

T Ambient temperature (°C)

u Mean transport velocity of alloy in viscometer (cm/s)

U Sliding speed of pad (m/s)

U_o Sliding speed of pad at liftoff condition (m/s)

W Vertical force on pad (N)

$\underline{W}$ Dimensionless load on pad

y Coordinate of vertical distance from bottom of drop

Z Head difference between mean entry meniscus and exit on viscometer tube (cm)

β Angle between horizontal plane and tangent to drop in vertical plane, also Arctan(dy/dr)

δ Density (Kg/m^3)

μ Viscosity (centipoise)

τ Surface tension (N/m)

θ Angle between tangent to surface and vertical direction measured in a vertical plane, also Arctan(dr/dy)

6. BACKGROUND

Direct current motors with superconducting field windings show great promise for marine propulsion as well as industrial and vehicular applications. Progress toward their utilization requires the development of current collectors with steady ratings near 3 Ma/m². Solid, high-metal-content brushes are of some interest; however, the greatest promise for low frictional and electrical losses is offered by liquid metal wetted current collectors. Principal interest in such systems has been devoted to annular rings, with the liquid held in place by centrifugal force. In a study of losses in such annuli, Brown, Riley and Sondergaard (1) have analyzed the magnetohydrodynamic flow in a channel with one moving wall and a magnetic field vector normal to that wall. They have offered a simple equation for the relationship of magnetohydrodynamic loss to Hartmann number, and this may be used for comparison of candidate liquid alloys.

In the investigation of a different approach to liquid metal wetted current collectors, the present authors (2) have reported an experimental study showing promise for individual brushes wetted by an alloy of gallium. Such brushes included alloy-wetted sandwiches made of porous copper braid compressed into a block. These showed considerable promise for applications where switching or other requirements call

for self-contained brushes. Similarly promising results were reported by Kostornov (3), using nichrome fibers. Much more promise was offered by spring-loaded tilted pads having the potential for hydrodynamic operation in the presence of the liquid metal. To assess these systems hydrodynamic and electrical behavior of the collector must be modeled, and this requires new data on alloy properties.

Reference (2) was concerned with an eutectic of Ga,In, and Sn which is liquid well below room temperature. Other alloys show comparably low melting points, and offer a considerable range of properties. For this reason, eutectics of Ga In Zn and Ga In Sn Zn have been included in the present study.

In a recent paper (4), Mitchan and Prothero have examined the relative problems of dry brushes and annular liquid metal current collectors. Their analysis appears favorable to the liquid metal current collectors, although they have only considered sodium/potassium eutectic as a working fluid. In their Table 3, they show the predominance of magnetohydrodynamic losses in 1 mm thick annuli, and the falling off of these losses as the film thickness is reduced to 0.1 mm. As a promising approach to achieve this advantage, they cite the hybrid system of Sondergaard, Reilly and Dilling (5), with a braid recessed into the annulus to

provide a compliant surface with an effectively thin film. As such it incorporates some of the features of porous metal blocks or crushed mesh pads.

Reference (2) continues the progression of configurations from porous pads to hydrodynamic pads. On the basis of the results reported there and the calculations offered here, such pads should be considered as a serious contender for low loss current collectors. Rings of compliant fingers may be visualized as attached to either the rotor or stator, and running on a thin liquid metal film.

Materials which might be considered for the conductive liquid include alkali metals and their alloys, mercury, gallium alloys and low melting solders. Low toxicity and room temperature liquidity both support the gallium alloys. Problems with these materials include the fierce attack on aluminum and zinc alloys, complex wetting behavior, and the need for property data. Despite warnings on the attack of solid surfaces by gallium, we were encouraged to undertake the earlier work and the present study by a report (6) where structural materials including a titanium-stabilized chromium-nickel stainless steel, copper and bronze were recommended for room temperature use after 1000-1500 hours of testing in a GaInSn eutectic.

Copper alloys were initially used by the present investigators (2) without noticeable deterioration. Yet Eriksson (7) has reported severe contamination of a Ga/In eutectic by dissolved copper in test times of 700 hours in the presence of copper surfaces. On the basis of his experiments, which he shows to be consistent with the data of (8,9,10), chromium appears to be an attractive and easily prepared surface, subject to low rates of attack. In Ref. (2) we have shown that spreading of GaInSn occurred without difficulty on chromium plated tool steel, and that slipper like contacts rode on this film with remarkably low contact resistance. We have retained these specimens and have observed them over two years of static storage while coated with the alloy, without damage visible at 20X magnification. A series of experiments on the copper-GaInSn system has been investigated further, and it has been shown that agitation plus current can lead to large amounts of dissolved copper in the liquid alloy, with the formation of a butter-like structure.

The adoption of GaInSn in the pilot study of Ref (2) was decided upon partially by the friction and wear results reported by Buckley, Johnson and colleagues (11,12). Viewing those studies in the present context, the principal finding is that friction and wear are low under conditions of

concentrated contact, and that there should be no fear of seizure or excessive wear should displacements in machines lead to pressure of sliding surfaces against one another. Friction and wear studies in the present study support this finding.

6.1 Low Melting Temperature Alloys

In Ref. (2) a number of promising low melting temperature alloys were listed, including an eutectic of GaInSn, with composition (in weight percent) of 62.5 Ga, 21.5 In, 16 Sn. This is the most commonly referenced eutectic. Reference (13) indicates that there is a second eutectic in the system with a closely comparable melting point. A third eutectic, with an even lower melting point is listed in Ref. (14). Table 6.1 lists these and other low melting eutectics beginning with the lowest melting temperature.

TABLE 6.1. COMPOSITION OF LOW MELTING TEMPERATURE ALLOYS BY WEIGHT PERCENT

	Ga	In	Sn	Zn	Melting Temp.	Ref.
A	61	25	13	1	3	(14)
B	62	25	13	-	5	(14)
C	62.5	21.5	16	-	10.7	(13,14)
D	69.8	17.6	12.5	-	10.8	(13)
E	67	29	-	4	13	(14)
F	75	24.5	-	-	15.7	(13,14)
G	82	-	12	6	17	-
H	92	-	8	-	20	(14)
I	95	-	-	5	25	(14,15)
J	100	-	-	-	29.75	(15)
					29.78	(16)
					29.92	(13)

7. LIQUID METAL LUBRICATED CURRENT COLLECTORS

7.1 Introduction

This research program has involved property measurements, and laboratory experiments on the behavior of metallic and carbon contacts wetted by gallium alloys, while they are conducting electric current. A concept, which arose early in the program was that of spring loaded brushes, operating as hydrodynamic tilted-pad bearings, with the

liquid alloy as lubricant. Questions as to whether such operation was feasible were raised at the initiation of the program. The principal questions concerned whether or not oxide films on the pad and slipring would impede current flow, and whether or not organic films from contaminants would form on the surfaces with similar deleterious effect. It was argued that a sliding brush could have some abrasive contact to remove such films, while hydrodynamic support would separate the surfaces and eliminate such abrasion.

The experimental program has established that pads can carry large current with very small voltage drop. These experiments were partially motivated by early experiments by the Navy, which found bad behavior, such as solidification, of gallium alloys in Couette-flow slip ring assemblies. With appropriate metallic surfaces such as copper, chromium and nickel we find that the alloys will remain suitable lubricants in a laboratory apparatus, operating with inert (argon) atmosphere. Material sources of failure were indentified as aluminum and zinc alloys, which are subject to rapid intergranular attack, and the formation of a black substance. This may have participated in the early failures. While the research reported here was under way, motor development was in progress at the David Taylor Research Center (Annapolis). The motor and generator configurations

use Couette flow slip rings, where a smooth rotor disk turns in a space bounded by two parallel disks (Fig. 7.1). A partial filling of this space with liquid metal leads to the liquid moving out to a concentric dam when the rotor disk is turning. The film around the outer elements of the disk serves to carry current from the stationary disks to the rotating disk. Problems of stability occur in such a configuration as a result of electromagnetic forces and hydrodynamic forces. These are moderated when the spaces holding the fluid are made thin. At the same time this leads to problems when the disk or stator materials distort mechanically or thermally, and rub.

One solution under development has been to insert a woven braid of plated copper in the gap space (Fig. 7.2). This provides some compliance, a sacrificial wear surface, and useful constraint on the fluid to improve stability. Evaluation of such a system is in progress. Its main benefits have been demonstrated. However, a general problem is anticipated in that it may prove too restrictive when large thermal expansion may occur owing to a rub.

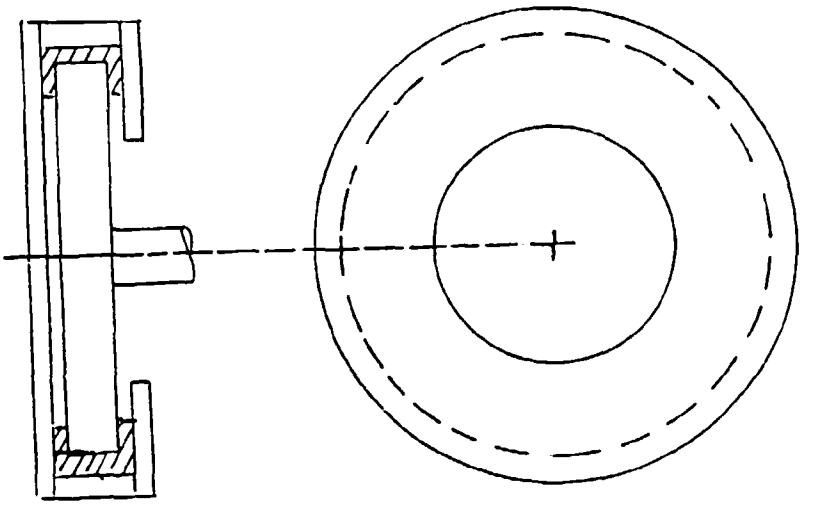

7.1 Couette Flow Current Collector

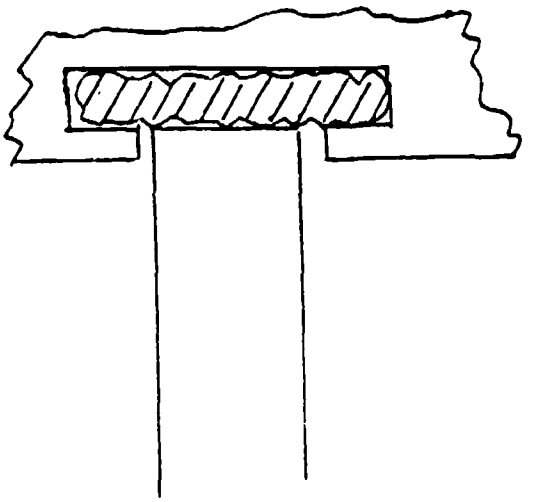

7.2 Braid Enhanced Current Collector

7.2 Spring Loaded Pads

An extension of the concept of hydrodynamic pads will offer the advantages of the braid, will offer large radial compliance, and will also offer a minimum of rubbing resistance. The innovation discussed here concerns the development of a ring of pads to be inserted into the flow space, where the braid now resides. It offers simplicity of manufacture, compliance, and amenability to operating in reverse and forward modes. The behavior of pads with liquid metal lubricant in the presence of current has been documented in Ref. (2). Calculated performance and behavior, based upon properties measured by the investigators, is reported in Ref. (20).

Figure 7.3 shows a direct replacement for the braid of Fig. 7.2. In cross section it is seen that a series of tines are partially cut from a band of conductive material, and formed into bent fingers. Figure 7.4 illustrates how a liquid metal film will support the finger against an elastic preload which results from an initial interference between the finger and the rotating disk. The figure also shows how the lift acts when the direction of sliding is reversed. The finger is shown as having a sharp bend, but in reality such a bend must have a radius of curvature. Indeed, the radius may

be generous or even predominant and still give rise for hydrodynamic separation of the surfaces under realistic loads and sliding speeds.

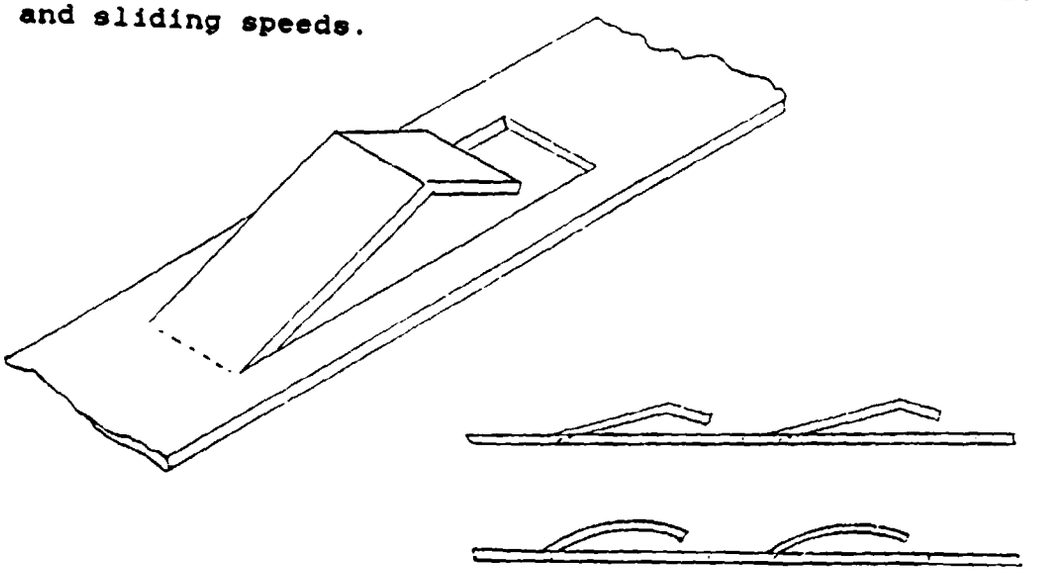

Fig. 7.3 Strip of spring loaded pads.

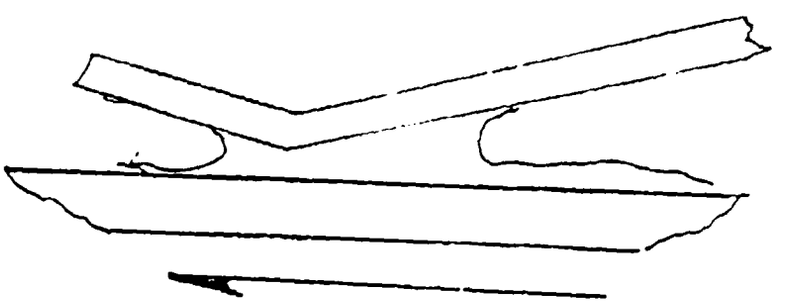

7.4 Illustration of hydrodynamic support

In the reverse direction of sliding as shown in Fig. 7.5 there is the possibility of intermittent dry contact where a sizeable coefficient of friction may arise. A lockup can occur unless the dimensions of the finger are selected to preclude this. The favorable condition is achieved when the combined friction and normal forces on the contact form a resultant which must passes below the attachment point of the finger on the band, as illustrated.

A variation of the configuration, which does not change its function, may be convenient for manufacture, assembly, and the achievement of higher numbers of pads on the ring. This is accomplished by cutting the band into segments which may be chosen to allow overlap of the fingers.

Long duration runs of such individual fingers, and pairs of these have been carried out in the reported program. These have been shown to run without deterioration of performance over 5-hour periods. Such runs have required the fingers to accomodate runout of about 0.03 cm requiring them to flex by such an amount at a rate of about 30 cycles per second. A broad range of loads up to the excessive load of 1 Kg have been applied to fingers under operation without adverse effect. Current has been operated steadily up to 300 amperes per contact pad (3 M-amp/m^2). No phenomenon was

discovered which would limit long term operation.

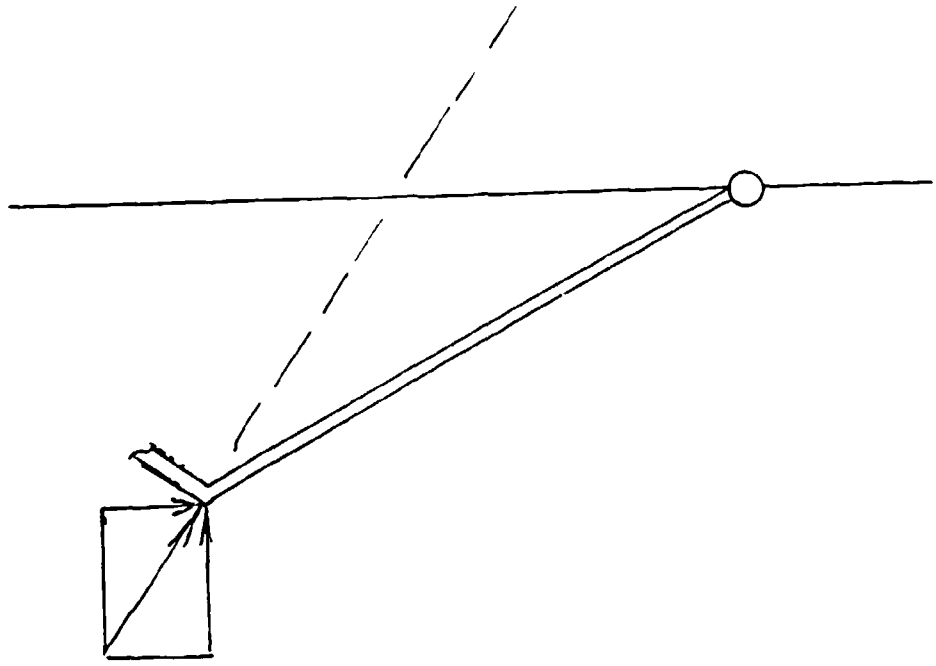

7.5 Forces on pad under reverse sliding.

Rings of pads as described above are not restricted to the stationary member of the slipring system, but may be carried by the rotor instead. They may be riveted, welded, brazed or screwed to this member or to the stationary member, and performance is not compromised relative to the assembly where the band is held in slots as illustrated above.

We believe this configuration will have immediate application in the superconducting, homopolar and related motors under study by the Navy, and can contribute to improved reliability, assembly, and performance.

8. EXPERIMENTAL PROGRAM

8.1 Surface Attack on Copper and Materials Compatibility

Eriksson (7) reports that GaIn binary eutectic dissolved copper in cathodic electrical contact. The result was embrittlement and the formation of a pulpy compound. He attributes the attack to the indium in the alloy, and he reports an estimated 17.6% by weight content of copper in the pulpy compound. Copper was used extensively in the experiments reported here. Because of this, specimens of copper in contact with GaInSn (for periods up to 3 years) were available for examination for attack. In day to day handling no significant attack of copper was observed. The formation of a semi-solid phase of oxidised GaInSn was observed but was not confined to copper specimens. However, in the presence of electrical current the formation of the semi-solid phase was more rapid for copper specimens. Because copper is a very common material in electrical and current collector systems the effects of GaInSn on copper called for detailed examination.

In laboratory observation of the action of GaInSn on copper in day to day handling and long term static exposure the stripping of all oxide by the eutectic from the copper

was observed to be very rapid. This naturally suggests the oxide layer on the copper may play the dominant role in the dissolution of the copper. The experiments devised tested this effect as well as provided a comparison to a working current collector. Because of the complexities of performing such a series of experiments in a functioning current collector an experiment was needed which provided the essential elements of such a current collector with greater ease for use in the laboratory. Accordingly the tests reported in this section consist of (1)long term static exposure of specimens which have been subjected to a variety of conditions including electrical current, (2)a current collector rig, and (3)a series of current collector and handling system simulations with newly devised test systems.

The long-term-exposure specimens were disks of steel which have been chromium or copper plated, a nickel crucible, stainless steel and copper test specimens, and galvanised steel jaws used to hold copper braid.

The current collector apparatus consisted of a copper cup, outer rotor of 100 mm diameter, and an internal stator with two copper finger contacts 6 mm wide and inclined to a line contact (See Fig. 8.1). Current was supplied from an arc welding transformer to the copper fingers via 6 mm bronze rods. In addition the stator contained copper filler tubes

for the eutectic alloy and for the argon gas supply. The bronze rods were not in contact with the GaInSn alloy. The feed tubing to the rig was Tygon B44-4X. A 6-conductor wire in the stator provided instrumentation output for contact resistance and current. The current collector itself had one end face of copper and one of clear Lexan to allow direct observation of the system in operation. The entire assembly was then sealed in a glass sided tank.

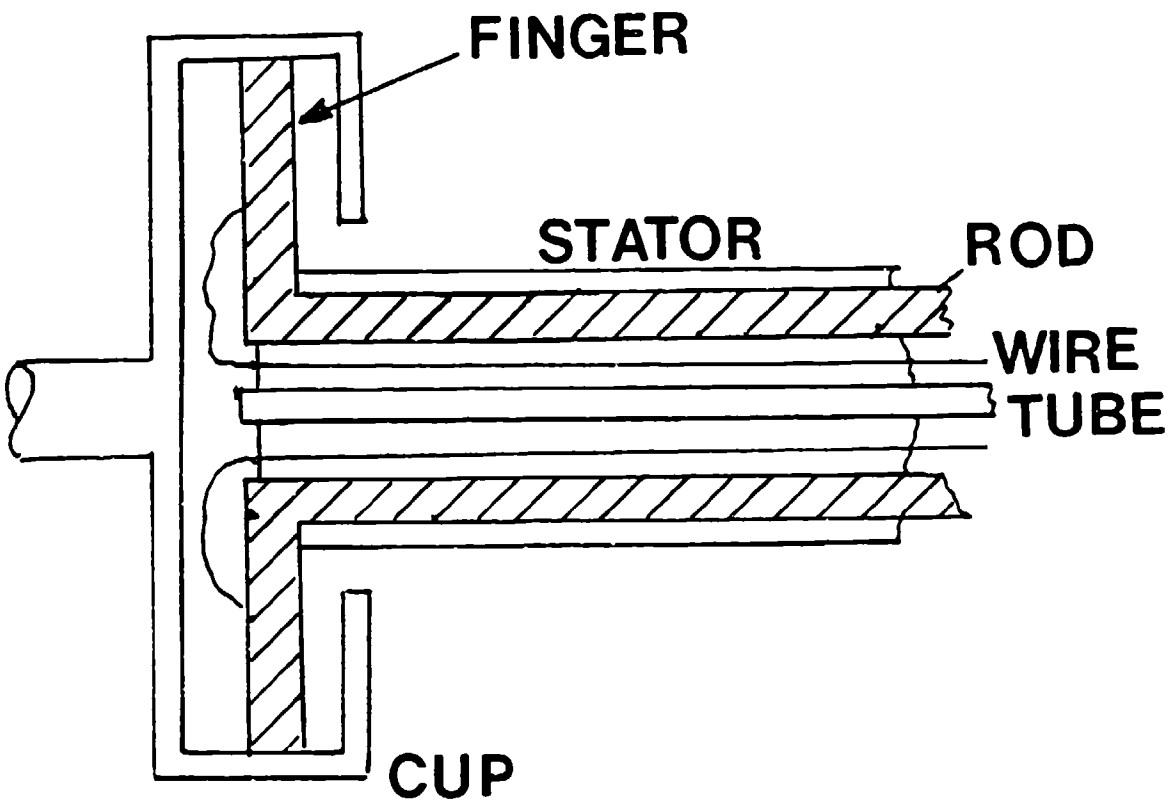

8.1 Simulated current collector

The alloy was pumped into the current collector via a rotary micropump when called for by rising contact resistance or sparking. Argon was used to purge the current collector itself and the glass enclosure to ensure a completely inert atmosphere prior to the admission of the GaInSn alloy and during the test runs. The result of these runs is shown in table 8.2.1.. A notable feature of these runs was the pause of 18 days between the first run and the final one, During this time the collector was left full of alloy and under an inert blanket, in the exact condition of termination of the first run. The initial run was terminated due to exhaustion of the available supply of GaInSn alloy. The second run was started exactly 435 hours later with a fresh supply of alloy. The most notable feature of the second run was that with the addition of a small quantity <10cc of fresh alloy to refresh the old alloy paste surface in the collector the collector was able to resume operation and required no additional alloy to be added during the run to maintain satisfactory operation. The second run was much longer than the first one, between required additions of alloy, and less than 1/5 as much alloy was required. The second run was also notable for much lower voltage drop across the contacts and up to 5 times the current density. The high current segment was limited by the overheating of the epoxy filler in the stator

The formation of a semi-solid paste in the collector annulus was observed at the end of the first run. This material was firm, and the pads ran on its surface and not that of the underlying copper. Thus a transition layer between the copper and the liquid alloy was created which exhibited very cood current collecting qualities. As can be seen in table 8.1. the copper content of this transition material was the highest measured at 800 ppm, although this is far less than the 17.6% by weight with GaIn (7). The semisolid material which was formed was not pasty but quite firm, retained indentations without surface recovery, and when broken exhibited brittle type seperation rather than the tearing seperation that might have been expected of a paste. The copper cup underlying the semisolid did not exhibit pitting or evidence of corrosive attack in low power microscopic examination. The fingers exhibited definite tip abrasion from the runs but showed no pitting and had not become embrittled.

The long term exposure observations are summed up in Table 8.2. No severe attack was observed except for the zinc coating on galvanised steel, and the aluminum peices. In both sustems the attack appeared to have reached its final extent and to not be ongoing. The Aluminum samples exposed to GaInZn showed much slower attack than those exposed to

GaInSn and GaInSnZn, although the final result was similar. For short term exposure anodizing was able to protect aluminum from attack from GaInZn. This may be an important handling requirement in some applications.

It cannot be overstressed that the attack of aluminum by GaInSn, and GaInSnZn is both rapid and catastrophic. The pitting observed on the copper fingers was in the region of the bend in the finger where tensile stresses would be the highest. The pits are few in number and shallow. There was no alloy in the pits which may have some other source than attack by the indium in the GaInSn.

The bench test was devised to meet several goals: (1) simulation an alloy supply and replenishment system, (2) atmosphere control, (3)cover fluid effects, alloy flow, (4) material exposure and compatibility, and (5)the effects of electrical current. It had to be able to simulate these variables singly or multiply as required to identify exactly how the systems that were modeled would perform. It had to allow visual observation and instrument monitoring. Because of the contamination and cleaning problems it had to be easily replicable and disposable.

The bench-test system that resulted from these considerations was simple, inexpensive, and self contained, and is illustrated in Fig. 8.2. The apparatus consisted of a

glass beaker, a stopper, and a magnetic stirrer. The glass beaker allowed visual monitoring and was free from chemical attack. The polymer stopper was easily penetrated by glass tubing for alloy, atmosphere, and cover-fluid introduction and by electrodes and instrumentation. The magnetic stirrer provided fluid motion to simulate pumping or current collector motion, the range of flow which can be provided ranges from barely detectable to frothing turbulence. The results of these experiments are shown in table 8.3.

In summary it can be said that attack of copper does take place in GaInSn, but it is of a much milder nature than reported for GaIn. The copper plating on the chromium plated tool steel specimens was not penetrated by the attack from the indium even though this plating was only a few micrometers thick. The reaction product may have a future as a current collector material in itself, as the runs on this material were the longest and most trouble free of the program. The attack on the copper is of smaller magnitude than the erosion of the copper from friction against the oxide of the GaInSn. The control of the oxidation of the alloy is a more major consideration for current collector operation in the short term, at least, than the corrosion of the copper.

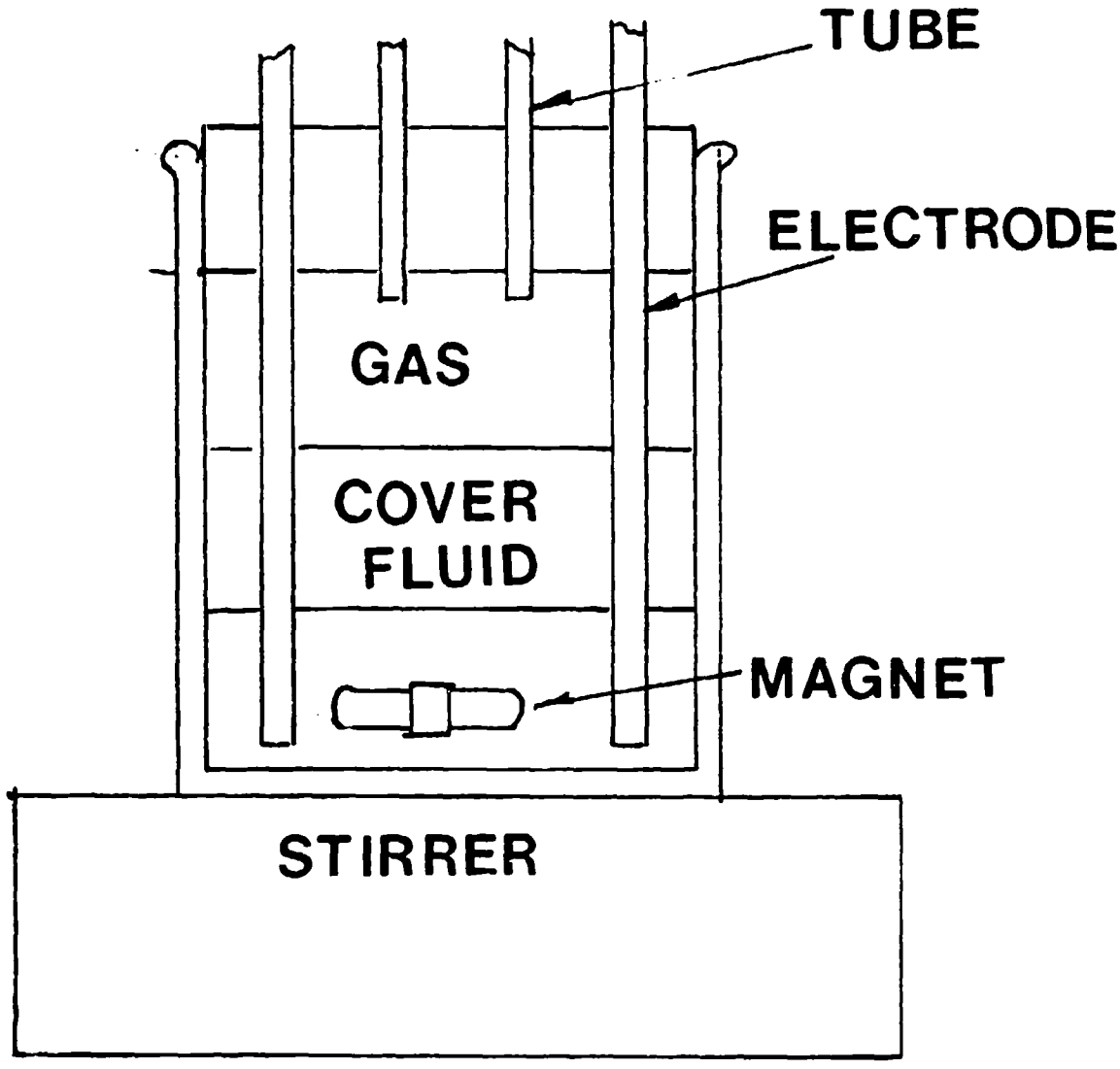

8.2 Bench-test for corrosion and compatibility simulation

TABLE 8.1. Current Collector Simulation (AT 1075 RPM)

Run #	Voltage Drop (volts)	Time (Minutes)	Current (amps)	Comments
1	Start up	7	52	
1	0.027	21	53	
1	0.025-0.026	30	53	
1	0.03	37	53	alloy added
1	0.023	38	53	
1	0.059	55	53	peak flash
1	0.023	56	53	alloy added
1	0.023	72	53	very steady
1	0.022-0.023	75	53	
1	0.023	78	53	constant flow
1	0.019-0.018	105	53	
1	0.023	150	53	steady reading
1	0.018-0.019	182	54	flash of 0.015V
1	0.017-0.017	230	55	current rising
1	0.013-0.016	240	55	sparks final reading
	18 day Static Period to Renew Alloy Supply			
2	0.004	0	52	startup
2	0.009-0.011	1	115	current raised
2	0.009-0.015	2	115	fluctuating
2	0.012	3	115	steady
2	0.020	5	173	current raised
2	0.029-0.028	7	270	epoxy of stator smokes
2	0.009	8	75	current lowered
2	0.009-0.010	10	75	
2	0.008-0.009	13	76	
2	0.008	13	77	
2	0.008-0.009	23	77.5	
2	0.008-0.009	28	77	
2	0.0014-0.0017	35	77.5	
2	0.029	41	77	
2	0.034	44	76	
2	0.036	48	77	
2	0.034	50	77	
2	0.036-0.038	53	76	
2	0.040-0.041	56	77	
2	0.040	62	77	
2	0.047	73	77	
2	0.051-0.052	82	78	
2	0.049-0.050	83	78	
2	0.049	88	78	
2	0.053	100	78	
2	0.055	101	78	sparks
2	0.082	101	78	current rising
2	0.056	101	78	blue sparks
2	0.078	102	78	final reading

TABLE 8.2. ANALYSIS OF SAMPLES FROM TEST CELLS AND CURRENT COLLECTOR

	Sample 1	Sample 2	Sample 3	Sample 4	Sample 5
Source	sump[1]	control	oxidised[2]	unoxidised[3]	collector[4]
In (%)	22.1	22.7	21.9	21.9	22.0
Sn(%)	16.0	16.4	15.7	15.8	16.0
Ag (ppm)	0.3	0.3	<5.0	<5.0	1.0
Bi (ppm)	5.0	15.0	15.0	15.0	15.0
Cd (ppm)	2.0	0.1	0.3	2.0	2.0
Cu (ppm)	50.0	10.0	30.0	50.0	800
Ni (ppm)	-	<1.0	-	-	-
Pb (ppm)	150	75	50	75	150
Th (ppm)	0.3	0.3	-	-	-
Sb (ppm)	-	-	-	10	-

[1] Sump alloy discharged as liquid from the current collector in tests, after a short exposure time to copper and current.

[2] GaInSn run with oxidized copper strips having 1 μm oxide film.

[3] GaInSn run with clean copper.

[4] Collector sample of semi-solid residue left in the current collector annulus after current runs of Table 8.1.

Table Note: Values above given in percent (%), are by mass spectrograph, all values in parts per million (ppm), are by atomic absorption.

TABLE 8.3. SUMMARY OF LONG TERM EXPOSURE SAMPLES

Run	Comments
1. Copper surface run with carbon brushes. (2.5 year exposure)	Electroplated copper surface on chromium plated tool steel. No pitting of thin plated surface observed. (NaOH and HCl applied, HCl faster cleanup of surface also removed CuO_2.)
2. Copper surface run with copper braids. (2.5 year exposure)	Electroplated copper surface on chromium plated tool steel. Same as Carbon on Copper.
3. Copper surface run with copper fingers. (2.5 year exposure)	Electroplated copper surface on chromium plated tool steel. Solid alloy on fingers, no pitting underneath. At 30X magnification some individual pits in copper adjacent to GaInSn in area where copper was bent over to form fingers (tension region). No pitting on copper electroplate.
4. Chromium plate (2.5 year exposure)	Chromium plated tool steel. Both HCl and NaOH stripped GaInSn completely from surface. Surface undamaged. HCL caused rusting through chromium plate.
5. Nickel Crucible (2.5 year exposure)	Wetted with GaInSn and had been uncleanable with NaOH. HCl completely stripped alloy from surface, particles of alloy suspended in HCl solution.

8.2 WETTING AND COMPATIBILITY

The wetting of surfaces by GaInSn depends very much on the oxide film covering the alloy. This oxide film as seen in the surface tension section has considerable strength. The oxide film also wets most materials except plastics. In order to achieve wetting it is usually necessary to smear the alloy on the surface to be wetted. This mechanical action breaks through the oxide fllm and allows new reactive metal to come into contact with the surface. Because of this it is necessary to provide a cover fluid or gas to prevent oxide from forming on the alloy. The best combination is a cover gas to prevent future oxidation and a cover fluid such as HCl or NaOH to remove the oxide film. this results in much improved wetting. The oxide of the material being wetted will usually then be reduced forming oxide in the GaInSn. This can lead to the formation of a second type of pulpy mass made up of oxidised GaInSn. This semisolid can be returned to liquid state by either HCl or NaOH which strip the oxygen from the GaInSn. Also 1,1,2 Trichloro 1,2,2 Triflouro ethane (Freon liquid) worked well in the laboratory to keep the alloy from becoming oxidized.

The Freon was preferred to the HCl and the NaOH because

both of these fluids posed corrosion problems of their own. The Freon was not as effective in keeping a reactive surface on the alloy but did not in turn attack the copper and stainless steel components as the HCl and NaOH. In early experiments to simulate a pumping supply system for a current collector alloy was recirculated by means of a rotary tubing pump through flexible tubing and copper tubing. With no cover fluid but only inert gas blanket the tubing clogged with pulpy material very quickly. The cover fluids not only helped to keep the liquid alloy liquid but also inproved the pumpability of the oxidized pulp by providing a fluid medium for the pulp to flow in. All of the cover fluids however attacked the flexible tubing which resulted in tubing failures and introduction of organic contaminants into the alloy. The performance of these experiments is summarized below in Table 8.3. In instances where the GaInSn alloy had wetted copper it was observed that it stripped the oxide from the copper. In the final series of experiments described above in section 8.2 a 10006 film was grown on aa pair of copper strips to be compared to a pair of same sized unoxidised copper strips. The oxide layer was removed during the assembly of the apparatus and before any effect could be measured. The time scale for assembly of the test jars was about 1 minute.

TABLE 8.4. COMPATIBILITY OF GaInSn WITH LABORATORY MATERIALS AT ROOM TEMPERATURE

GOOD	Chromium*, Nickel*, Copper*, Polyethelyne, Polystyrene*, Polypropylene, Rubber*
POOR	Halogens, N_2O_4, $HgBr_2$, S, Acetonitrile, Strong Oxidizers, Bases

* Exhibits good wetting.

GaInZn exhibits milder attack than GaInSn, on aluminum:

1. Old Thick Oxide reduces attack.
2. Anodizing reduces attack.
3. Light Oxide is penetrated by attack from alloy.
4. Fresh Metal is rapidly attacked and disintegrates.

TABLE 8.5. PERFORMANCE OF CIRCULATING SYSTEMS FOR GaInSn IN FREON

Tubing Type	Flow Rate (ccs/min)	Duration to Failure of Tubing (hours)
Tygon R3603	3	72
Tygon B-44-4-X	3	72
C-Flex	3	14
Viton	3	0.62
Norprene	3	2.5
Silicone	3	0.50

Table Ncte: All tubing 0.8mm inside diameter.

In table 8.5. the Tygon tubing formulations showed the longest life. Their failure coincided with the clogging of the tubing and the termination of flow due to blockage of the flow pasages. A similar experiment was run using NaOH and an Argon blanket which survived much longer in fact 1092 hours. In spite of this long life the corrosion of the copper in the circulating system from the NaOH was deemed to make the system unacceptable. By contrast a non-pumping system of Freon and GaInSn and copper survived for 2016 hours without corrosion being observed in the copper.

8.3 Viscosity Measurements

Viscosity was measured at room temperature by timing flow through a capillary tube. The arrangement is

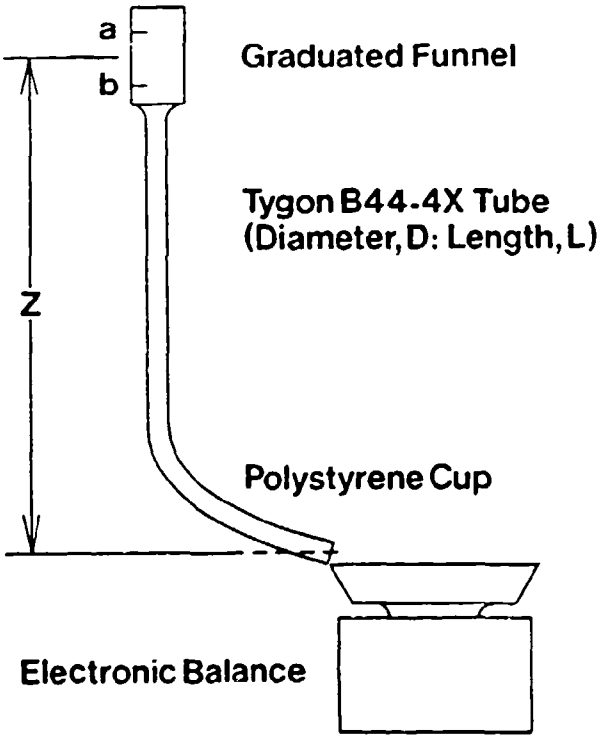

8.3 Viscometer.

illustrated schematically in Fig. 8.3. The tube was made of Taigon B-44-4X. Flow originated in a graduated cylindrical funnel. The discharge from the tube was received in a cup on a digital balance. After flow was initiated, the balance was tared and a stopwatch was started simultaneously when an upper graduation was passed by the meniscus in the inlet funnel. When the meniscus passed a second graduation, the time was taken and the balance was read simultaneously. The head Z was measured from a point halfway between the two graduations, which were approximately 1 cm apart. The procedure and calculation were checked with runs using water, and gave a viscosity of 0.888 at 22 C, which may be compared

with a handbook value (16) of 0.91. This suggests that the cumulative error in measurement of weight, time and dimensions is approximately 0.025.

Calculations were based upon the following equations, adapted from Ref. (17). The continuity equation is used to calculate mean flow velocity in the tube:

$$u = (m/\pi)/(\delta \; t \; r^2) \qquad (8.1)$$

To calculate the equivalent pressure drop on the tube,

$$p/\delta = (Z \; g - u^2) \qquad (8.2)$$

Here the kinetic energy term as represented by u^2 is not $u^2/2$, because, as Ref. (17) points out there are two losses of magnitude, $u^2/2$, these being the kinetic energy discharged, and the loss in going from uniform velocity profile to parabolic profile at the tube entry. In all cases the u^2 correction was small, comprising only about 1.3 % of the term in parentheses in Eq. (8.2). Using the above calculated quantities, the kinematic viscosity is given by:

$$\mu/\delta = [(p/\delta) \; r^2/ \; 8 \; L \; u] \; 10^8 \qquad (8.3)$$

Once kinematic viscosity is known, Reynolds number may be calculated to provide confirmation that the flow is fully in the laminar range.

$$Re = (\delta/\mu) \; d \; u \qquad (8.4)$$

Typical measurements are listed in Table 8.6.

TABLE 8.6. VISCOSITY DATA

Material	T	L	Z	D	m	t
GaInSn	24	42.4	30.53	0.080	10.0	24.63
GaInZn	23	42.5	30.53	0.080	4.84	8.4
GaInSnZn	23	42.5	30.53	0.080	5.4	8.4

Calculated results are summarized in Table 8.7.

TABLE 8.7. CALCULATED VISCOMETRY RESULTS

Material	GaInSn	GaInZn	GaInSnZn	Water
u (cm/s)	12.426	16.50	19.54	19.89
p (N/cm^2)	29765	29647	29549	39784
μ/δ (centistokes)	1.127	0.8452	0.711	0.888
Re	88	156	219	179

The above reported technique was adopted because of special difficulties in working with gallium alloys. Glass could not be used because the gallium wets glass easily and makes reading of positions of free surfaces impossible. The polymer chosen was not wetted. Being transparent, it permitted reassuring observations that slugs or bubbles were not forming in the fluid. Repeated experiments assured that the results were valid to two significant figures, for the fluids as tested. The fluids themselves were received from the supplier under seal with argon gas.

A careful review of the above measurements will show that Eq. (8.2) gives a result that is virtually independent of the velocity correction, and is dependent mainly on the mass and time measurements. Because we had larger quantities of the GaInSn available, the mass and time were extended, so this measurement was the most precise. The order of magnitude of the result was not greatly different for the three materials.

To convert to absolute viscosity, a density, δ, must be supplied. Although we are able to measure densities of conventional fluids to better than 0.1% error, difficulties were encountered in applying the same techniques to the gallium alloys. The first measurements showed undertainties possibly exceeding 5%. A series of repeat tests was undertaken in 1988, using sections of the tubing that was employed in the viscosity expriments. These have led to the conclusion that the density differences of the three alloys were indistinguishable, and that a density of 6.4 g/cc is the best value for the materials as supplied.

Table 8.8 shows comparative data for μ for the three alloys and Table 8.9 shows data for some representative molten metals.

TABLE 8.8. VISCOSITIES OF CANDIDATE LIQUID METALS

Material	μ, centipoise
GaInSn	7.22
GaInZn	5.42
GaInSnZn	4.55

TABLE 8.9. VISCOSITIES FOR OTHER LIQUID METALS

Material	μ, centipoise	Ref.
Ga	1.9	(13)
Hg	1.55	(13)
Sodium Potassium Eutectic (NaK)	0.47	(13)

8.4 Resistivity Measurements

Resistivity was measured by placing a calibrated resistor, R_1, in series with a column of the chosen alloy See Fig. 8.4). The column was made of Taigon B-44-4X, which was found to have long-term compatibility with the alloys. The cross section of the tube was circular, and the diameter was precisely equal to the manufacturer's nominal diameter to better than one percent accuracy, as confirmed by photomicrographs.

Table 8.10 summarizes data for the three eutectics at low current levels. Plots of resistivity versus temperature for other liquid metals show only a weak rise with temperauture, as compared with conductive solid metals. As a

check on the instrumentation, a wire of OFHC copper was substituted for the column. A handbook value for annealed copper is close to the measured value, thus providing reassurance in the system. Handbook values (13) are listed in Table 8.11 for pure metals which may be of interest.

TABLE 8.10. RESISTIVITY MEASUREMENTS (at 22°C)

Material	L (cm)	d (cm)	R_1 (ohm)	e_1 (v)	e_2 (v)	R_2 (ohm)	r (μ-ohm cm)
GaInSnZn	100	0.080	9.9	16.9	237	0.7058	35.4
GaInZn	50	0.080	9.9	7.5	244	0.3039	30.55
GaInSn	100	0.080	10.0	19.1	263	0.726	36.48
Cu	100	0.064	510.1	2.4	466	0.052	1.70

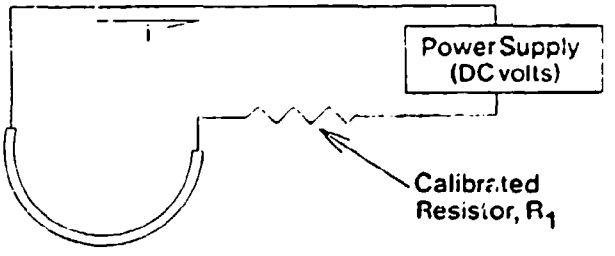

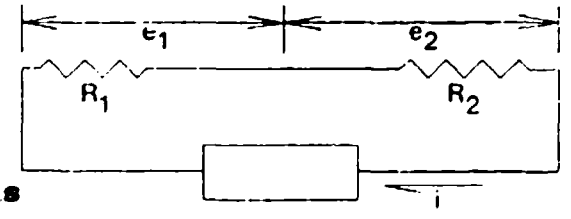

8.4. Resistivity Apparatus

TABLE 8.11. RESISTIVITY OF PURE METALS

Material	Reference	r
Cu	(16) at 20C, annealed	1.724
Ga	Ref. (13), 26C	25.9
In	Ref. (13), 154C	29.1
Sn	Ref. (13), 231C	47.6
Zn	Ref. (13), 419C	35.3
Hg	Ref. (13), 50C	98.4
NaK	Ref. (13), 50C	37.5

The values for resistivity of the alloys are not far from those of the pure elements in the liquid state. Confidence is reinforced by the observed good behavior of the alloy in filling the tube. For resistivity of binary GaIn alloys, see also Pashaev, Pashaev, Chalabov and Revelis (18).

8.5 Surface Tension

Surface tension plays an important role in the stability of liquid metals in Couette flow current collectors. Because data were unavailable for the alloys of interest, measurements were undertaken. An experimental procedure was developed that only requires tiny amounts of sample alloys. It has the additional advantage that the data may be treated analytically in a process which guarantees that the reported

magnitudes are accurate.

For eutectics of GaInSn, GaInZn and GaInSnZn, room temperature measurements are reported for surface tension, τ, based upon a pendant drop technique. The results are significantly lower than recently published data of Migai (21), for the GaInSn eutectic. However, a difficulty has been discovered in application of the bubble technique as used by Migai, and this serves to provide a partial explanation of the differences in results.

The evolution of our analysis procedure is discussed. The final procedure employs two independent calculations. One exploits a force balance on a pendant drop to provide a magnitude of surface tension. The second calculation generates a complete surface contour for the drop, using the calculated surface tension. This may be compared with the physical contour as a test of accuracy.

Using this technique, we have analyzed a large number of photographs of drops, including a special set of repeat runs made on the alloy of principal interest, GaInSn, in which special care was exercised on all aspects of the experimental formation of drops in inert atmosphere. These results along with a conservative estimate of error sources should serve to establish our data as the appropriate values of surface tension to be used in the fluid mechanical analysis of

Couette flow current collectors.

8.5.1 Candidate techniques for measuring surface tension. A pendant drop technique was selected for the measurement of surface tension of the alloys under investigation. The choice was dominated by knowledge that liquid gallium and gallium alloys exhibit an unusually tough oxide film that mechanically influences surface behavior. A technique that generates a fresh surface in a short time interval was required. Of the techniques considered the following were included:

Capillary Rise. The difficulty of reading a meniscus in a wettable capillary presents a practical difficulty. The fact that no new surface is generated in the measurement is a more serious problem in view of the above mentioned oxidation, and influence of the oxides upon wetting (2,7).

Du Nuoy. Surface aging is the principal problem in this technique, where a ring is pulled upward through an already formed surface.

Bubble Pressure. This procedure is commonly used with molten metals. It generates new surface by blowing bubbles at the tip of an inverted tube immersed in the liquid. Maximum pressure before the bubble separates is used to calculate surface tension. This technique has been employed

by Migai (21). It offers the disadvantage that the bubble cannot be observed visually.

Pendant Drop. This was selected because new surface is generated with each drop, and all essential measurements are displayed in a directly observable form. It offers an additional advantage of being adaptable to very small quantities of material (10^{-3} cc).

To accomplish the measurement, a capillary tube was pointed vertically downward into the interior space of a flat-windowed absorption cell. A positive displacement pump displaced liquid metal down the capillary and into a drop that hung from its tip. The drop was photographed with an appropriately calibrated lens system, using a camera mounted on an optical bench along with the cell. From the elevation-view (side-view) of the drop, sufficient information could be calculated to give volume below any horizontal datum plane that cuts the droplet. Pressure on the plane could be calculated by several techniques, and a balance of forces could be used to provide magnitudes of the surface tension force acting on the datum plane.

To find the hydrostatic pressure in a liquid at a point immediately beneath a surface, one must relate this to the surface tension and two components of curvature, measured along orthogonal axes in a plane tangent to the surface.

This pressure can be calculated from drop contours in the immediate vicinity of the ring where the datum plane cuts the surface, or pressure be calculated elsewhere, and related to that on the datum plane by the laws of hydrostatics.

In applying the pendant drop technique it is not necessary that the drop be at the point of breaking loose when the measurement is made. Except with GaInSn, great care was required to form a stable drop.

8.5.2 Difficulties with the bubble pressure technique.

The bubble technique is often used to measure the surface tension of liquid metals because it may be applied without great difficulty to hot metal in a crucible. A vertical tube is extended a distance Z below the surface of the liquid, and gas pressure is raised slowly inside the tube. Initially the meniscus is forced down to the outlet of the tube, and has a large radius of curvature. Hence it supports a small pressure difference between the interior and the fluid. As the pressure rises the bubble becomes more rounded until it is close to hemispherical shape, with vertical tangents at the points of attachment to the surface. In this condition the pressure is maximum, since further addition of gas must increase the radius of the bubble. In that case, taking a datum plane as the exit plane of the

capillary tube, where liquid pressure may be defined as zero, the preɑsure of the gas p above the liquid pressure is:

$$p(\pi r^2) = 2 \pi r \tau \qquad (8.5)$$

or

$$p = 2 \tau / r \qquad (8.6)$$

Migai states the exterior diameter of his capillary tube, but not the inside diameter. Furthermore, he avoids the necessity of specifying how the bubble attaches itself by calibration of the system with mercury, a fluid of documented surface tension. The maximum pressure is related to the surface tension by a linear multiplier, or calibration coefficient. The tube used by Migai is kovar, and it is not known or discussed as to the contact angle shown by mercury and gallium alloys against this material or its oxidized surface.

Figure 8.5 Shows a schematic crossection of the capillary tube wall, with the meniscus to the left. In the upper diagram, a material havinng positive contact angle (wetting) is shown, with the capillary bore to the left. The meniscus moves down the tube, beneath the gas G. When it reaches the corner, it moves to a point where the slope of the tube accomodates simultaneously: (1)a vertical meniscus at attachment, and (2)the characteristic contact angle. Any further addition of gas can accomplish enlargement of the

bubble by bulging it out below the point of attachment, thus causing an increase radius and a drop in pressure. By the above argument the bubble radius for the wetting material would be expected to be the inside radius of the tube, R_1.

In the lower diagram of Fig. 8.5, a fluid that shows negative contact angle is illustrated. The meniscus is initially concave downward. As it reaches the end of the tube it can navigate the turn and remain relatively flat, while preserving the characteristic contact angle. Further gas addition will cause the contact point to move radially outward, along the flat surface. When it finally reaches the

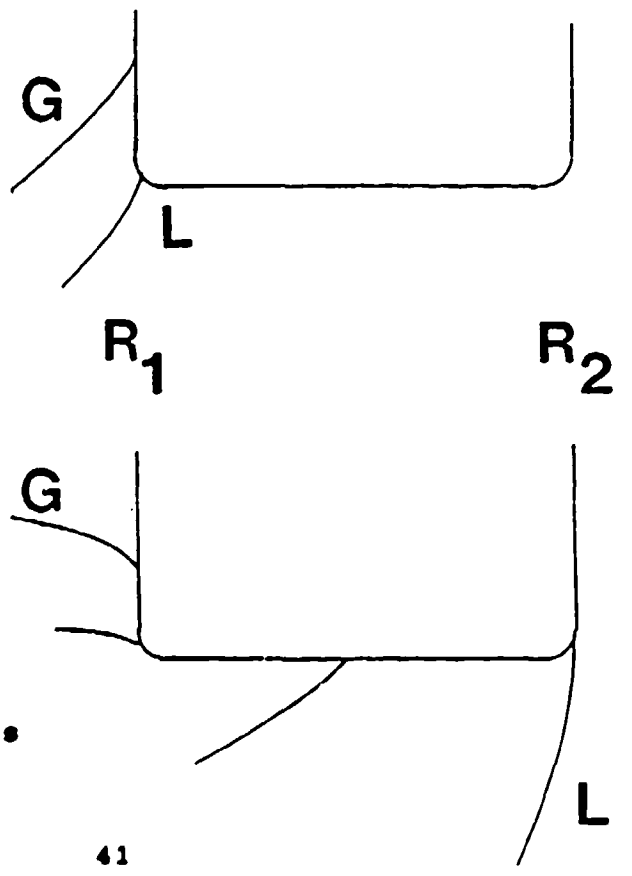

8.5 Contact angle effects

outer corner it becomes effectively pinned, moving around to a point where the characteristic contact angle prevails along with a vertical meniscus, and the radius for pressure calculation is R_2.

If the calibration were done with such a non-wetting fluid, showing a negative contact angle then:

$$\tau_{nonwet} = K\ p = p(R_2/2) \tag{8.7}$$

For the wetting alloy it would be

$$\tau_{wet} = p(R_1/2) \tag{8.8}$$

From Eq. (8.7) it is seen that the calibration coefficient for the nonwetting material is:

$$K = R_2/2 \tag{8.9}$$

If this were applied to the wetting fluid alloy, then Eq. (8.7) would require:

$$\tau_{wet} = K\ (R_1/R_2)\ p \tag{8.10}$$

The uncorrected use of the nonwetting calibration coefficient for the wetting fluid would overestimate the surface tension of the wetting fluid by the ratio R_2/R_1.

Because, mercury, and the gallium alloys all may show anomalous wetting behavior, measurements of surface tension by the bubble technique must be viewed with caution. At the same time, the variation with temperature would be expected to be accurately represented, if contact angle remains constant under temperature change.

8.5.3. Surface tension computation based upon curvatures at datum plane.

Figure 8.6 shows a drop of GaInSn, with several important variables identified. A datum plane cuts the drop near the point of attachment. The quantity d_s represents the diameter of the circle formed where the drop surface intersects the datum plane. The quantity r_s represents the radius in the elevation view of the surface at the point of intersection with the datum plane. The quantity r_o represents the radius of curvature at the lowest point on the drop, and V represents the volume of the drop below the datum plane.

In general the pressure beneath a point on a surface can be expressed as:

$$p = \sigma (1/r_a + 1/r_b) \qquad (8.11)$$

where r_a and r_b are radii of curvature of the surface measured in two planes which are mutually orthogonal and are each orthogonal to a plane tangent to the point on the surface beneath which th pressure p acts. To find the pressure where the datum plane cuts the surface in Fig. 8.6, one of the radii can be identified as r_s which is measured in the plan-view provided by the droplet photograph. The second practically identifiable radius is $d_s/2$. Because the datum

plane is not, in general, orthogonal to the surface, being inclined by the angle θ, it follows that the curvature in a plane orthogonal to the surface and orthogonal to the photograph is given by:

$$1/r_n = (2/d_s)(\text{Cos}\theta) \qquad (8.12)$$

When the datum plane cuts an almost vertical filament then Cos θ is near to unity.

The pressure in the fluid on the datum plane must, by hydrostatics, be uniform, since the plane is perpendicular to the gravity vector. It is given by:

$$p = \tau[(1/r_s) + (2/d_s)\text{Cos}\theta] \qquad (8.13)$$

The vertical pressure-force acting on the drop at the datum plane is:

$$f_p = - p\ (\pi\ d_s^2/4) \qquad (8.14)$$

The negative sign for the pressure force indicates that the force acts downward for positive pressure. In Eq. (8.13) the curvature is positive when the radius of curvature lies inside the fluid. When the datum plane is made to pass through or near an inflection point in the plan view, the quantity r_s is infinite. As a practical matter, the diameter d_s can be measured precisely, whereas the radius r_s is found by projection to an intersection of two perpendiculars to the surface near to the point where curvature is to be measured. Although the measurement of r_s is not prohibitively

difficult, the finding of the inflection point (near which $1/r_s$ is small) appears at first to be a less difficult alternative. If so, it would be computationally advantageous to select the datum plane so as to pass through the inflection point in the photograph of the droplet.

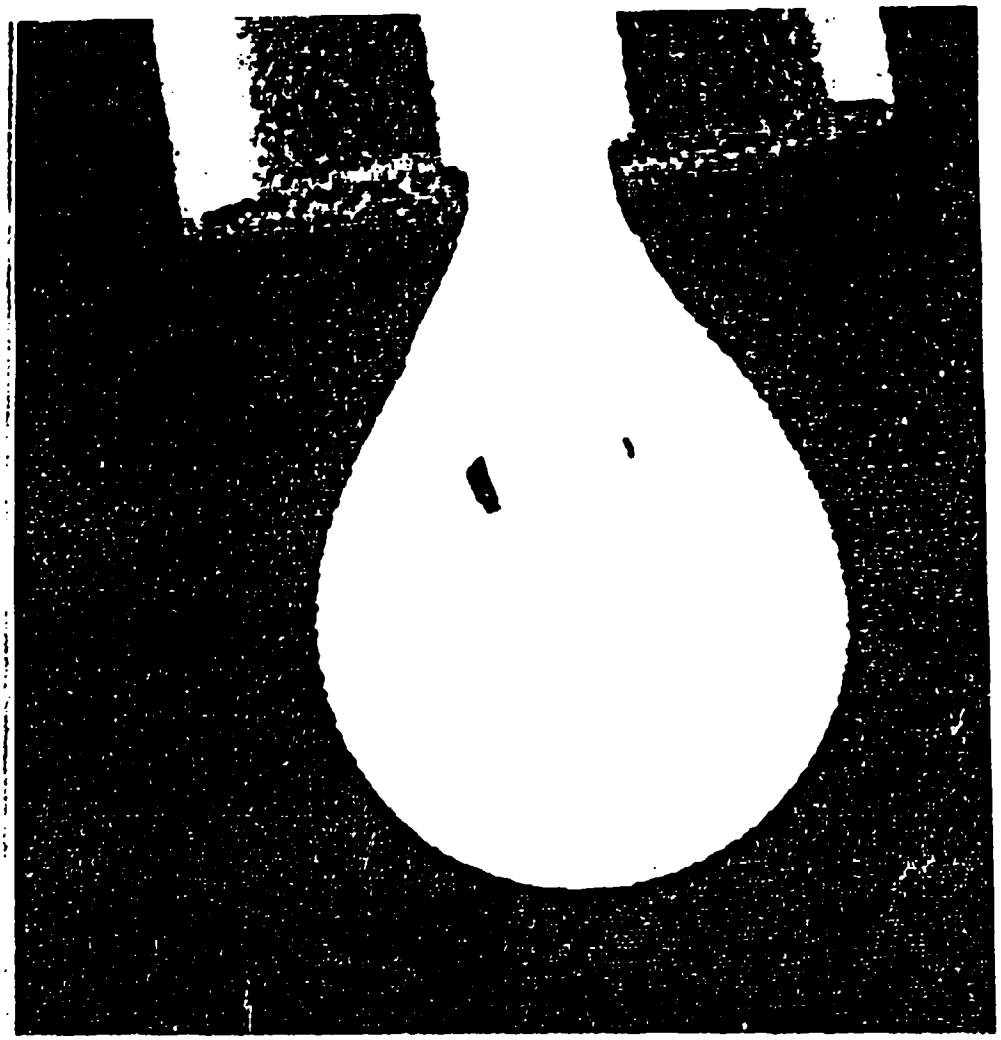

Fig. 8.6 GaInSn Drop

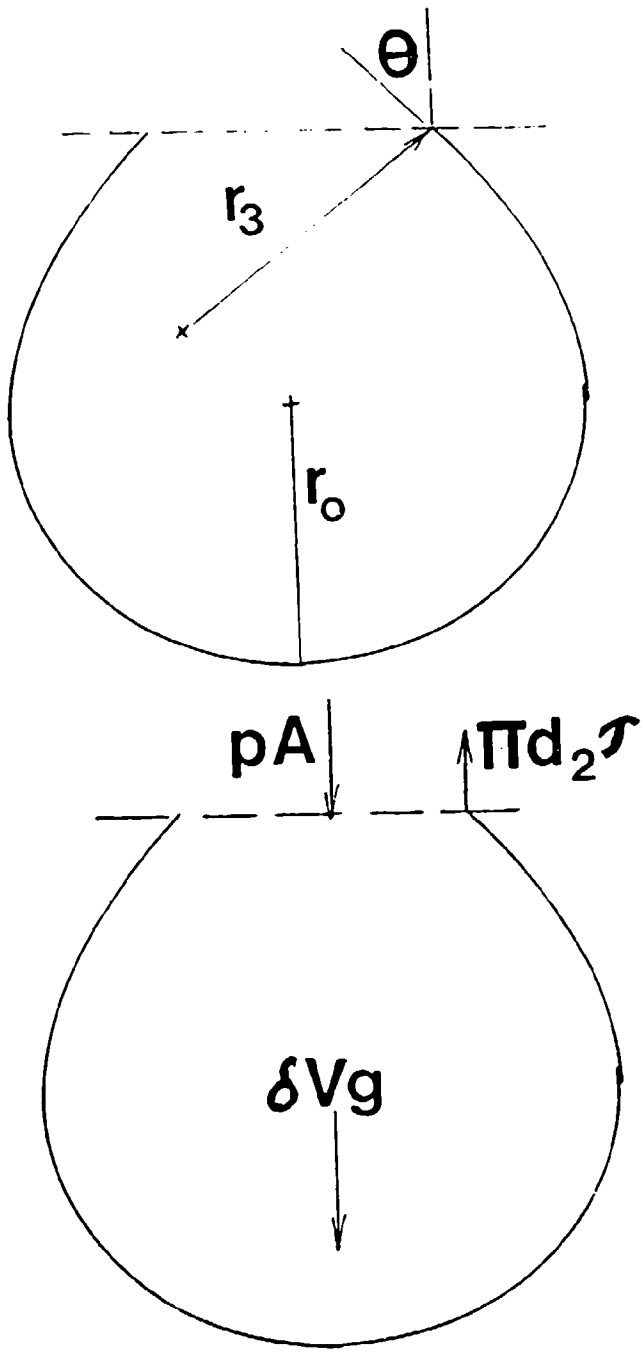

Fig. 8.7 Force balance

As shown in Fig. (8.7), the surface tension force acting upward on the ring where the datum plane cuts the surface is:

$$f_\tau = \pi\, d_2\, \theta \qquad (8.15)$$

The net force on the datum plane is the sum of the surface tension force and the pressure force, and is given by:

$$f = (\pi/4)d_2^2[-(\sigma/r_3) - (2\tau/d_2)\mathrm{Cos}\theta] + \pi d_2 \tau \mathrm{Cos}\theta \qquad (8.16)$$

Simplifying:

$$f = \pi d_2 \tau[-d_2/4r_3 + \mathrm{Cos}\theta\ /2 \qquad (8.17)$$

If the volume below the datum plane is V, and the density is δ, then equilibrium requires that:

$$\tau\, d_2[(d_2/r_3)\ [\mathrm{Cos}\theta\ /2 + d_2/4r_3] = g\ V\ \delta/\pi \qquad (8.18)$$

Figures 8.8 show a photograph of a droplet, and are representative of the repeatedly observed differences in measurements on the alloys. The three materials showed qualitataively different behavior in the experiment. The GaInSn drew into a large drop on a straight neck. For the GaInZn and the GaInSnZn, the neck is short.

Values of surface tension, calculated from Eq. (8.18) were found to be variable upon small changes of the location of the datum plane. Careful review of all calculations showed that the magnitude of r_3 was important, and inaccurate to evaluate. The inflection point proved to be difficult to locate also, and the range of reasonable positions gave rise to significant changes in the predicted surface tension.

These difficulties suggested that, although correctly formulated, the evaluation of pressure from surface curvatures in the datum plane was not a practical approach to accurate surface tension values.

8.5.4. Volume calculation.

In the calculation presented above, and in the selected calculation scheme presented below, the volume of the drop below the datum plane is required. Several approaches were made toward finding a simple method for estimating this volume. These included generation of a theoretical curve for the surface and finding a best fit. With experience these were abandoned, and a direct method was applied, where the photograph of the drop was printed onto a grid, oriented with precisely vertical and horizontal lines. This grid served to divide the drop into a stack of disks, and for each an upper and lower radius could be measured. The volume of a disk would be:

$$dV = [\pi (d_2^2 + d_1^2)/2]dy \qquad (8.19)$$

Here d_1 is measured on one plane and d_2 is measured on the plane above it. The volume would be the sum of these beginning at the lowest point of the drop and continuing upward until d_2 corresponds to the datum plane. To check the accuracy of this procedure two tests were made, one being for

the error produced be breaking a sphere into discrete disks, and the second being reading error in determining the diameters. Table 8.12 summarizes the effect of discretization, using exact values for the diameters. In this table N is the number of disks, and V is the precise volume.

TABLE 8.12. VOLUME ESTIMATION FOR A SPHERE (V = 11494.04)

N	Calculated, V_c	Error$[V - V_c]/V$
6	10656.28	0.072
13	11272.03	0.019
27	11436.97	0.0049

We may conclude that once the number of divisions is well above 13 we may expect roughly a 1% error from discretization alone. A more critical test was to draw circle to represent a sphere on the same grid as used for the drops, and use the same procedures for reading the diameters at points where the sphere crosses grid-lines. Table 8.13 summarizes the results.

TABLE 8.13. SPHERICAL VOLUME CALCULATED FROM READINGS ON A DRAWING

N	Volume Calculated, V_c	Error
6	10424	0.093
13	11007	0.042
27	11150	0.029

Table 8.13 shows a combined discretization error and reading error. For the experimental drops approximately 50 divisions were used, bringing the combined error to approximately 1%.

8.5.5. Improved calculation procedure.

The pressure in the drop at the datum plane was represented in Eq. (8.13) in terms of two components of surface curvature at the datum plane. An improved pressure calculation uses the curvature at the bottom of the drop to give the pressure at that point, and applies hydrostatics to relate pressure elsewhere in the drop to this quantity, p_o. By this approach the pressure at any elevation, y, measured from the lowest point in the drop is given by:

$$p_y = 2\tau/r_o - \delta g y \qquad (8.20)$$

Writing the equivalent of Eq. (8.18) for equilibrium, using the above pressure:

$$[2\tau/r_o - \delta g y]\pi d_s^2/4 + g V \delta = \tau \pi d_s \mathrm{Cos}(\theta) \qquad (8.21)$$

Regrouping:

$$(\tau/g\delta)(\pi d_s \mathrm{Cos}\theta - 2/r_c) = (V - \pi y d_s^2/4) \qquad (8.22)$$

It is convenient to introduce a scale factor σ, which permits the linear dimensions to be measured in arbitrary units on the droplet photograph such that

$$r_{photo}\,\sigma = r \qquad (8.23)$$

where r_{photo} is measured in tenths of an inch in the present study, and r is the true dimension in meters. It is convenient to define a parameter G as follows:

$$G = \tau/\delta g\,\sigma^3 \qquad (8.24)$$

and

$$G = [V - \pi\, y\, d_s^2/4]/[\pi d_s \mathrm{Cos}(\theta) - 2/r_c] \qquad (8.25)$$

This may be used directly with the photographic representation of the drop, with an arbitrarily selected datum plane for evaluation of V, d_s and θ.

8.5.6 Alloy Density.

Because only small amounts of the GaInZn and GaInSnZn alloys were available, the chosen technique for density measurement was to fill capillary tubes with the alloy and weigh them. Tygon B44-4X was found to be suitable in that the capillary interior was precisely the nominal value of 0.8mm, when measured in a microscope, for typical cut crossections. The exterior could be wiped clean, and did not

tend to retain a gallium film as did glass. In addition the filament of alloy could be observed to determine if it filled the tube fully. The results of measurement were somewhat surprizing in that the room temperature densities of the three alloys were the same within the scatter of the measurement. This quantity was found to be 6.4 g/cc at 20°C. Migai has reported a value of 6.358 at 25°C. He notes a deviation of individual measured points of 0.5%, and thst d δ/ dT = - 0.00044. This would project to a magnitude of 6.36 at 20°C. This would constitute only a 0.62% deviation from our measurement.

8.5.7. Numerically generated drop shape.

The same general relationships employed in Eqs. (8.13) and (8.20) can be combined to provide a scheme for computation of drop shape. For this purpose we may express the curvature component in the elevation view of the surface as:

$$d\beta/ds = 1/r_s \qquad (8.26)$$

Nomenclature is illustrated in Fig. (3.14). Here we have defined a new angle β so as to avoid confusion with the previously defined θ. The quantity β is defined as the angle between the tangent to the surface and the horizontal plane, at a given r,y point. The curvature as defined in Eq. (8.26)

requires that the radius of curvature extend into the fluid. Combining the two components of surface curvature one finds, as in Eq. (8.13):

$$p = \tau(\mathrm{Sin}\beta/r + d\beta/ds) \tag{8.27}$$

Here ds is an element of arc length on the surface, measured in the plane of the photograph. It follows that:

$$dy = \mathrm{Sin}\beta\ ds, \text{ and } dr = \mathrm{Cos}\beta\ ds \tag{8.28}$$

Drawing upon Eq. (8.20), which also gives pressure at a given y, we find:

$$\tau(d\beta/ds + \mathrm{Sin}\beta/r) = (2\tau/r_o - gy\delta) \tag{8.29}$$

Rearranging and introducing the varible G as above:

$$d\beta = (2/r_o - \mathrm{Sin}\beta\ /r - y/G)ds \tag{8.30}$$

With a suitbly defined scale factor contained in G, the angular and linear quantities are as directly measured in the drop photograph. Upon choice of a suitably small ds, the

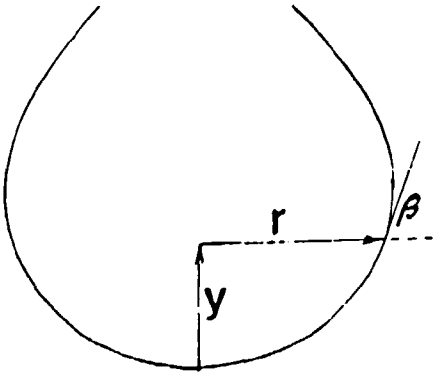

8.9 Nomenclature for synthesis of drop shape.

equation may be integrated from an origin at the bottom of the drop where initial r = 0, and $\beta = 0$. The quantity $\mathrm{Sin}(\beta)/r$ becomes ambiguous at the origin, but reference back to the definition of curvature would require it to be such that at y = 0:

$$\mathrm{Sin}\beta / r = 1/r_o \qquad (8.31)$$

For a typical photograph r_o = 20 units, and a practical ds = 0.1.

8.5.8 Application of the analysis to a specific drop.

Figure (8.8) shows a drop of GaInSn arbitrarily chosen from the most recent series, and designated R3. From this figure, the measurements listed in the appropriate column of Table IV were taken. These quantities were measured by a micrometer caliper on the drawing and are expressed in multiples of 0.1 in. units. A reference dimension was included in the photograph, and the scale factor was determind to be:

$$\sigma = 6.896552 \times 10^{-6} \ \mathrm{m/unit} \qquad (8.32)$$

Letting the quantity $g\delta = 62524\ \mathrm{N/m^3}$, the above quantities were inserted into Eq. (8.25), and the folowing results were obtained:

$$G = 11496.587; \quad \tau = 0.4451341\ \mathrm{N/m} \qquad (8.33)$$

As a check on the validity of this result, the magnitudes of G and r_o were transferred to Eq. (8.30), and the contour of the drop was calculated. The calculated quantities in Table 8.14 resulted.

TABLE 8.14. MEASURED AND CALCULATED DROP CONTOUR

Dimension	Measured	Calculated
r_o	1.975	1.975*
d_{max}	41.6	41.44
y_o	48.62	48.62*
d_s	18.15	18.25
Θ	0.58	0.5792

* Experimental value inserted into calculation

Since there is such close agreement between the drop shape used to obtain G and the synthesized drop shape based upon that G, we may conclude that it represents an accurate value. On the basis of the above discussion, the density is known to 0.6%, and the scale factor was measurable at least this accurately, the value of τ listed in Eq. (29) is an accurate one for the GaInSn material used, at T = 21°C.

8.5.9 Results for a series of drops of GaInSn.

Data for a series of drops of GaInSn are collected in Table 8.15. Calculated τ is shown at the right. Measurements are presented in units of tenths of an inch on the photograph. The scale factor is 6.896×10^{-5} meters/unit.

TABLE 8.15. DATA FOR A SERIES OF DROPS

	d_{max}	r_o	d_a	y_a	θ	V	τ
R1	41.6	19.5	21.5	47	0.61	44061	0.4429
R2	42.25	20.5	17.7	49.2	0.54	45546	0.419
R3	41.9	20.1	17.35	49.4	0.58	45263	0.453
R4	44.15	18.85	20.35	48.25	0.56	49934	0.518
R5	42.55	19.0	17.43	49.91	0.59	43159	0.460
R6	42.25	19.6	18.45	48.25	0.59	43411	0.434
R7	42.6	18.75	19.85	46.95	0.62	44176	0.497
R8	42.0	20.02	16.12	48.75	0.61	42025	0.452
R9	40.7	19.35	19.8	45.0	0.63	38162	0.[illegible]4
R10	42.5	21.05	23.45	45.4	0.56	44700	0.348

Mean	0.440
rms error	0.0465
σ of mean	0.0147

TABLE 8.16. SUMMARY OF SURFACE TENSION RESULTS

Material	Temperature T (°C)	Surface Tension τ (N/m)
GaInSn	21	0.440
GaInZn	21	0.466
GaInSnZn	21	0.333
GaInSn in air	21	0.564

TABLE 8.17. DATA FROM OTHER SOURCES

			Ref.
Ga	30	0.735	(13)
In	170	0.34	(13)
Sn	300	0.526	(13)
Zn	510	0.785	(13)
GaInSn	25	0.533	(6)

8.5.10 Summary.

The three materials showed measured surface tensions with closely comparable magnitudes. We would conclude that none has a special advantage in this respect. The measurements show that the alloys have reduced surface tension relative to pure gallium. For GaInSn the measurements

of Migai, show a magnitude eleveted above ours by approximately 25%. We believe that the range of errors innherent in our measurements could not account for the discrepancy, and offer our value is the better one. Using data from Migai for dt/dT we find a change of -0.0256 for a 200 °C temperature rise. This indicates that the change of surface tension over the range of operation in current collectors is negligible.

9. RESULTS AND DISCUSSION

9.1 Predicted Performance of Current Collectors

In Ref. (1) the magnetohydrodynamic power dissipation is given by the equation:

$$p^*_{ry} = 2/3\ k^3\ M^3 \qquad (9.1)$$

where M is the Hartmann number and is given by:

$$M = B_o y_o (1/\underline{r}\ \mu)^{0.5} \qquad (9.2)$$

Equation (9.1) is valid for channels where the aspect ratio ranges from 5 to 10, where aspect ratic is axial width of channel divided by radial gap. Fluid properties appear only in the group $1/\underline{r}\ \mu$, which becomes the appropriate figure of merit for comparison of candidate fluids, and appears to the first power in Eq. (9.1).

Table 8.8 summarizes the appropriate properties of the gallium alloys and two other candidates. The quantity $1/\underline{r}\ \mu$ has its lowest value for Ga/In/Sn, indicating that this fluid would experience the least magnetohydrodynamic loss. Sodium potassium eutectic is the least attractive fluid by this measure.

9.2 Tilted Pads

In Ref. (2) the authors discussed the possibility of using hydrodynamic-pad brushes with the Gallium Alloys, as these had performed well in the initial experiments. Two questions must be asked relative this application: (1) When does the pad lift or become hydrodynamic, and (2) what is the friction loss? Bearing theory may be applied determine these. Equations for performance of an inclined pad are given by Cameron in Ref. (19), and are rearranged here for convenient interpretation.

$$U/W = (h_o/B)^2/(6\underline{W}\ L\ \mu) \qquad (9.3)$$

and:

$$F/U = [(\mu BL)/h_o][Ln(K+1)\ /K] \qquad (9.4)$$

where U is the sliding speed, W is the load, $\underline{W}$ is the dimensionless load, and h_o is the minimum lubricant film thickness. Here K is the inclination ratio, given by:

$$K = (h_1 - h_o)/\ h_o \qquad (9.5)$$

Cameron shows that the optimal inclination ratio K is near unity, and for this the dimensionless $\underline{W}$ is

$$\underline{W} = \mathrm{Ln}(2) - 2/3 \qquad (9.6)$$

For the set of conditions listed above, values in Table 9.1 permit performance comparisons for the candidate fluids. Lift-off may be defined as the condition when calculated $h_o = 10^{-4}$cm. With the additional conditions that load W = 5N, and that B = L = 1 cm, the values of U_o the lift-off speed and F_o the friction force at lift-off may be calculated. These magnitudes are listed in Table 9.2, where it is seen that Ga/In/Sn provides the lowest lift speed for the alloys considered. Note also that the friction force, F_o, at lift is essentially the same for all of the candidate materials, and is quite small. The experiments in Ref. (2) showed that a pad of the type discussed could carry 3 M a/ m² without distress. Hence 333 pads could carry 10,000 amperes.

TABLE 9.1. LIFT OFF SPEED AND FRICTION FORCE

Alloy	U_o/W	U_o	F_o/U_o	F_o
	cm/N-s	cm/s	N-s/cm	N
GaInSn	.00872	.436	.00500	.00218
GaInZn	.0116	.58	.00376	.00218
GaInSnZn	.0138	.69	.00315	.00217
Ga	.0331	1.65	.00132	.00219
Hg	.0402	2.01	.00107	.00216
NaK	.134	6.70	.00033	.00218

An additional equation for tilted-pad performance concerns the Joulean dissipation in the lubricant film. For the pad where K = 1, the resistance of the liquid metal film for a single pad is:

$$R = \underline{r}\, h_o/0.69 \qquad (9.7)$$

Table 9.2 has been prepared, by drawing upon Equations (9.3,9.4,9.5,9.6,9.7), for the special case of pad load, W = 1 N. This was chosen because large loads, typical of monolithic brushes are not necessary to hold light, flexible fingers in contact with the slip ring. The rate of energy dissipation from friction Q_f, and that for Joulean dissipation is given by Q_J.

$$Q_f = F\,U \;;\quad Q_J = i^2\,R \qquad (9.8)$$

An additional figure of merit is the Reynolds number:

$$Re = \delta\,U\,h_o/\mu \qquad (9.9)$$

Turbulent transition is not as well defined for pads as it is in long tubes, being dependent on a length Reynolds number in the direction of flow as well as the thickness Reynolds number of Eq. (9.9). Furthermore, current and magnetic fields tend to stabilize the flow. Nevertheless, one would expect a lower bound of transition in the vicinity of Re = 3000.

TABLE 9.2. CALCULATED PERFORMANCE OF TILTED PADS

Ga/In/Sn (for K = 1, W = 1 N, B = L = 1 cm, i = 300 amp)

U	h	Q_f	Q_n	Re
(m/s)	(mm)	(Watt)	(Watt)	
1	0.03	0.014	0.015	30
2	0.05	0.021	0.022	86
4	0.07	0.029	0.031	244
8	0.09	0.041	0.043	692
16	0.13	0.058	0.061	1958
32	0.18	0.082	0.086	5538
64	0.27	0.116	0.122	15666

for the chosen dimensions the frictional and Joulean dissipation are nearly equal. At 64 m/s sliding speed the Reynolds number is clearly in the turbulent range. For the lower sliding speeds, film thickness is small, and could be provided by a thin film of the alloy on the slipring. For a ring of 333 pads conducting 10000 amp, $(Q_r + Q_j)$= 39 Watt.

9.3. Discussion and Recommendations

The data taken for gallium alloys are shown to represent reasonable magnitudes for viscosity and resistivity when compared with data from the literature for the component elements, and for similar alloys. One measure of Joulean dissipation in a magnetohydrodynamic Couette flow is $1/r\mu$. This combination of properties is shown in Table 8.8 to have a most favorable magnitude for Ga/In/Sn eutectic. This figure of merit is important in a flow where the Joulean dissipation is large relative to viscous dissipation.

The viscosity data have been applied to answer a question left unanswered in Ref. (2): "When would tilted pad brushes be expected to be supported hydrodynamically?" With reasonable assumptions, the lift-off speed was found to be very low relative to expected operating speeds. Additional calculations for tilted pads show film thickness during

operation to be small over a broad range of speeds. Power dissipation from friction and electrical heating are small over a realistic range of speed and current.

The Ga/In/Sn eutectic continues to show promise as a current collector fluid for reasons other than its low melting point alone. The calculations of performance of this fluid in tilted pads suggests that such a configuration may ultimately be atractive as a primary current collector configuration, or as an enhancement in an annular configuration.

10. REFERENCES AND BIBLIOGRAPHY

1. S. H. Brown, P. J. Reilly, N. A. Sondergaard: Magnetohydrodynamic Liquid Metal Flows and Power Losses in a Rectangular Channel With a Moving Conducting Wall, Journal of Applied Physics No. 62, 15 July 1987.

2. R. G. Burton, R. A. Burton: Gallium Alloy as Lubricant For High Current Density Brushes, IEEE Transactions Volume 11 No. 1, March 1988.

3. A.. Kostornov, V. D. Zozulia, V. Sin'kov, M. S. Shevchuk: Antifriction Materials Employing Fibers and Liquid-Metal Lubricants, Poroshkovia Metallurgiia, July (1973) pp. 22-26

4. A. J. Mitcham, D. H. Prothero: Pulse Current Colection For a Self Excited Homopolar Generator: Solid Brushes or Liquid Metal, 1987 Current Collector Conference Proceedings, University of Texas Press.

5. N. A. Sondergaard, P. J. Reily, V. Dilling: Investigations of Continuous Duty Ultra-High Current Density Sliding Contacts Utilizing Liquid Metal in Narrow Gaps, 1987 Current Collector Conference Proceedings, University of Texas Press.

6. L. L. Migai, T. A. Taritsyna, M. I. Taishcheva: The corrosion resistance of constructional materials in Ga/In/Sn eutectic, Nauchn. Tr. Nauchno-Issled. Proektn. Inst.

Redkomet. Prom-st., (840) (1978) pp 26-29

7. Jarl-Thure Erikson: Superconducting Homopolar Machinery: Liquid Metal Current Collection And Design Principals, 1982 Thesis, Tampere University of Technology, Finland.

8. S. P. Yatsenko, Yu. A. Anikin, Z. N. Dieva: The Corrosion of Group VIII Metals in Liquid Gallium, Fiziko Khiminicneskaya Mekhanika Materialov, Volume 8 1973, USSR.

9. S. P. Yatsenko, Yu. A. Anikin: The Corrosion of Group V Metals in Liquid Gallium, Fiziko Khiminicneskaya Mekhanika Materialov, Volume 6 1970, USSR.

10. S. P. Yatsenko, Yu. A. Anikin: The Corrosion of Group IV Metals in Liquid Gallium, Izv. Akad Nank. SSSR. Metal, Number 4 1970, USSR.

11. Thomas J. Kuczowski, Donald H. Buckley: Friction And Wear of Low-Melting Binary And Ternary Gallium Alloy Films In Vacuum And Argon, NASA Technical Notes D-2712, March 1965.

12. D. H. Buckley, R. L. Johnson: Gallium-Rich Films as Boundry Lubricants in Air And in Vacuum to 10^{-9} mm Hg., ASLE Transactions Volume 6, 1-11, 1963.

13. C. R. Tipton, Ed.: Reactor Handbook Volume 1, 2ND Edition, Interscience Publishers, New York, NY, 996-999.

14. Alfa Catalog, Morton Thiokol, Alfa Products Division, Danvers, MA, Y-109.

15. Form No. 102-321-10-83-05, Indium Corporation of

America, Utica, NY, pp 14-17.

16. R. C. Wheat, Ed.: Handbook of Chemistry And Physics, 67TH Edition, CRC Press, Boca Raton, FL (1987).

17. L. Prandtl: Applied Hydro- and Aeromechanics, McGraw Hill Book Company, New York, NY, 24.

18. B. P. Pashaev, D. K. Palchaev, R. I. Chalabov, V. G. Revelis: Electrical resistance of Ga/In alloys in the solid and liquid phases, Fizika Metallov Metallovedenie 3, (1974) pp 525-528

19. Alastair Cameron: Basic Lubrication Theory, John Wiley & Sons Limited, New York, NY, pp 48-55.

20. R.G. Burton and R.A. Burton, Properties and performance of gallium alloys in sliding contacts, Ragnar Holm Electrical Contacts Conference, IEEE, San Francisco, September 1988.

21. L. L. Migai, Experimental study of surface tension and density of gallium indium tin alloy, Russ. Journal of Physical Chemistry, 55, 1981, pp 1539-1541.

11. ACKNOWLEDGEMENT

This work was sponsored by the Office of Naval Research under the direction of Dr. Donald Polk, scientific officer. We also wish to express our thanks to Dr. Neal Sondergaard and his group at the David Taylor Research Center for their support and advice.

ENCLOSURE NUMBER 1
CONTRACT DATA REQUIREMENTS LIST
INSTRUCTIONS FOR DISTRIBUTION

DISTRIBUTION OF TECHNICAL REPORTS AND FINAL REPORT

The minimum distribution of technical reports and the final report submitted in connection with this contract is as follows:

ADDRESSEE	DODAAD CODE	NUMBER OF COPIES UNCLASSIFIED/UNLIMITED	NUMBER OF COPIES UNCLASSIFIED/LIMITED AND CLASSIFIED
Scientific Officer	N00014	1	1
Administrative Contracting Officer	S1103A	1	1
Director, Naval Research Laboratory, ATTN: Code 2627 Washington, D. C. 20375	N00173	1	1
Defense Technical Information Center Bldg. 5, Cameron Station Alexandria, Virginia 22314	S47031	12	2

If the Scientific Officer directs, the Contractor shall make additional distribution of technical reports in accordance with a supplemental distribution list provided by the Scientific Officer.

Distribution of Reports which are NOT Technical Reports

The minimum distribution for reports which are not technical reports is as follows:

ADDRESSEE	DODAAD CODE	NUMBER OF COPIES UNCLASSIFIED/UNLIMITED	NUMBER OF COPIES UNCLASSIFIED/LIMITED AND CLASSIFIED
Scientific Officer	N00014	1	1
Administrative Contracting Officer	S1103A	1	1